Conference on Modelling Fluid Flow (CMFF'15)
The 16th International Conference on Fluid Flow Technologies
Budapest, Hungary, September 1-4, 2015

INVESTIGATING THE ACCURACY OF DIFFERENT FIDELITY NUMERICAL METHODS FOR MODELLING THE AERODYNAMICS OF A BOX-WING AIRCRAFT

Csaba JÉGER[1], Dániel KUTROVICH[2], László NAGY[3]

[1] Department of Aeronautics, Naval Architecture and Railway Vehicles, Budapest University of Technology and Economics. E-mail: csaba.jeger@gmail.com
[2] Department of Aeronautics, Naval Architecture and Railway Vehicles, Budapest University of Technology and Economics. E-mail: k.dani1992@gmail.com
[3] Corresponding Author, Department of Fluid Mechanics, Budapest University of Technology and Economics. Bertalan Lajos u. 4 – 6, H-1111 Budapest, Hungary. Tel: (+36-1)-463-3465 Fax: (+36-1)-463-3464 E-mail: nagy@ara.bme.hu

ABSTRACT

This paper deals with the aerodynamics of a box-wing (a type of closed-wing) aircraft. As demand for long-endurance long-range unmanned aircraft is still rising rapidly, closed-wing designs could provide a cheaper, smaller and more efficient solution. Current literature on the topic mostly omits the deeper aerodynamic analysis, and instead opts for low-fidelity methods. Research of this unconventional wing shape is important to design, build and maintain aircraft for higher range, endurance and lower price. Computational Fluid Dynamics (CFD) analysis with high resolution methods is carried out on a small test aircraft. The investigation starts from Reynolds-Averaged Navier–Stokes (RANS) simulations with Shear Stress Transport (SST) turbulence model, and continued with higher accuracy Large Eddy Simulation (LES) and Detached Eddy Simulation (DES) models. Adaptive meshing is used for increased accuracy and performance. Numerical results are then compared to wind tunnel tests. The lift coefficients calculated and measured were particularly well matched. Pressure and shear stress distributions around the wings produced very similar profiles with every model.

Keywords: RANS, DES, LES, box-wing, nonplanar wing, UAV

NOMENCLATURE

Symbols

b	[mm]	wingspan
c	[mm]	chord length
c_L	[-]	lift coefficient
c_D	[-]	drag coefficient
I	[%]	turbulence intensity
m	[g]	mass
l	[mm]	length
u	[m/s]	flow velocity
S	[m^2]	wing area projected to the xy plane
t	[%]	airfoil thickness
γ	[°]	wing sweep angle
ψ	[°]	vertical connector sweep angle

Subscripts and Superscripts

ref	reference
L, D	lift, drag

Abbreviations

CFD	Computational Fluid Dynamics
SST	Shear Stress Transport
RANS	Reynolds Averaged Navier-Stokes
LES	Large Eddy Simulation
DES	Detached Eddy Simulation
VLM	Vortex Lattice Method
UAV	Unmanned Aerial Vehicle
AOA	Angle of Attack
GIS	Grid Induced Separation
IDDES	Improved Delayed Detached Eddy Simulation
CG	Centre of Gravity
RMS	Root Mean Square
FTN	Flow-Through Number

1. INTRODUCTION

The box-wing configuration is an unconventional nonplanar aircraft wing layout with several attractive properties. Theoretically it has the highest span efficiency due to the reduced induced drag and structural loads are also favourable compared to an equivalent planar wing. The wings form a closed loop and are connected to the fuselage on the front and rear of the vehicle.

A small test aircraft with a box-wing layout was designed and built along with a reduced-size model for wind tunnel measurements. The polar diagram of the aircraft was acquired for a fixed airspeed using multiple CFD methods and compared to data from subscale tests. Figure 1 shows the constructed aircraft during a test flight.

Figure 1. Small box-wing UAV in flight.

There is a well-developed literature available on the preliminary and conceptual design of nonplanar aircraft particularly box-wing configurations, for example in [1] and [2]. Low-fidelity Vortex Lattice Method (VLM) codes are employed in a number of recent works to enhance the accuracy of concentrated-parameter calculations, such as in [3]. Frediani et al. [4] [5] used the ANSYS Fluent solver for the RANS simulations of a proposed box-wing passenger aircraft.

It was suggested by Spalart et al. [6] that Detached Eddy Simulations are specifically effective on wing flow problems given that RANS simulations are not accurate enough and LES simulations have higher computational cost.

2. PROBLEM DESCRIPTION

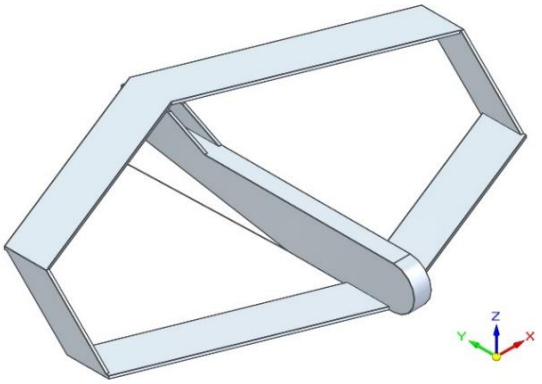

Figure 3. Test aircraft geometry.

For the ease of construction the aircraft has a very simple geometry which can be seen on Figure 2. It is powered by a small electric pusher engine which is omitted from both the CFD model and the wind tunnel mock-up. The wings are constant chord, 6% flat-plate profile along with the inverted vertical stabilisers and the rear wing mount. The forward and rear wing segments have inverted sweep angles, forming a rhomboidal (diamond) shape. The rear wing segments are offset from the forward segments along the vertical axis. The aircraft was made primarily from 6 mm depron sheet which is a commonly used material for models of this size. Principal dimensions and data are summarised in Table 1.

Table 1. Aircraft data

m [g]	b [mm]	l [mm]	S [m^2]
298.0	1000.0	650	0.2

γ [°]	ψ [°]	c [mm]	t [%]
68,20	45	100	6

The investigation is carried out on a fixed airspeed of 5.1 m/s and between the angle of attack (AOA) range of -1 and 6 degrees in the wind axes for the RANS simulations with 1 degree increments and in the 0° and 6° points for the DES and LES simulations.

3. NUMERICAL METHOD

The CFD model is the half of a parabola revolved around the Y axis with half of the aircraft imprinted in it as the problem is considered symmetric in the XZ plane. With this shape the angle of attack could be changed without mesh modifications.

Mesh generation was done in the ANSYS ICEM 14.5 commercial meshing software. An

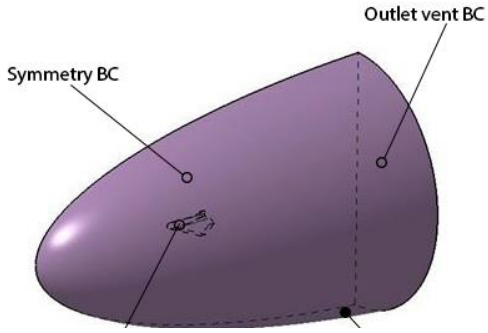

Figure 2. Flowfield with the boundary conditions.

unstructured tetrahedral mesh was used which was refined in the wake region of the wing and around the aircraft. The CFD simulations were carried out using the ANSYS Fluent 14.5 commercial software.

For the computations, hexahedral cells in a 15-layer thick boundary layer were used to ensure well-resolved wall modelling. The y+ value on the surface was below 1 in every instance.

The pressure-based SIMPLE scheme was used with second order discretisation. RANS simulations

used the standard two-equation Menter SST turbulence model, without the energy equation.

Mesh sensitivity studies were conducted with 3 meshes with 7.9, 8.5 and 11.2 cells. For the RANS and DES simulations, the second mesh (8.5 million cells) was used, LES simulations ran on the third mesh (11.2 million cells).

3.1. Large Eddy Simulations

For LES computation the literature usually suggests the use of high accuracy schemes [7] [8]. The need for them can be understood considering the properties of low order numerical schemes. Writing the partial differential equation modified by the numerical scheme, it can be found that for the case the scheme has accuracy less than 2^{nd} order a dissipative term is appearing. This term can be also called viscous term with numerical viscosity, because the effect is similar to the viscous dissipation. This viscosity is scaling with the square of the cell size, which means has a very similar form to the turbulent viscosity of the Smagorinsky model [9]. This fact explains why it is important to avoid the presence of such term in the solution. Using dissipative scheme it is impossible to distinguish between by the model and by the scheme produced dissipation. And the judgement of the result becomes difficult.

Other important requirement is for numerical schemes, that they should be stable, in the meaning that they do not amplify numerical errors. This requirement is usually in contradictory with the previous requirement especially for unstructured solvers [10] [11] [12].

The LES simulations used the incompressible implicit second-order finite volume method with a collocated grid arrangement implemented.

3.2. Detached Eddy Simulations

The Detached Eddy Simulation was originally developed for massively separated and high Reynolds number flows [13] for this reason it was a feasible candidate for this work. DES is a hybrid method where the near-wall regions are resolved with a RANS approach while the rest of the flow is treated with a LES method. DES was formulated with a number of the turbulence models and for this work the two-equation Menter SST model was used. The original formulation (often referred to as DES97) produced a premature and unphysical separation in certain cases, which is called Grid Induced Separation (GIS). The effect affects problems with thick boundary layers and shallow-angle separations and is caused by the DES limiter switching to LES mode which produces a stress depletion which in turn lowers skin friction, causing the separation. To combat GIS the modified model called Improved Delayed Detached Eddy Simulation (IDDES) was used which modifies the DES length scale (d) to preserve the RANS mode in the boundary layer. The coupled RANS model was the SST k-ω model.

4. WIND TUNNEL MEASUREMENTS

Measurements were carried out for comparison with the numerical results in the Blackbird 1 wind tunnel of the Department of Fluid Mechanics at the Kármán Tódor Fluid Dynamics Laboratory. The M=1:4 scaled-down model was 3D printed and surface-treated to create a smooth and accurate test article. Model dimensions can be found in Table 2.

Table 2. Scale model data

b [mm]	c [mm]	l [mm]	S [m^2]
250.0	25	177	0.0125

This small blower-type wind tunnel has interchangeable test sections in sizes of 0.35×0.35 m, 0.4×0.5 m and 0.15×1 m cross section which could be closed or opened (from to the laboratory atmosphere). The 0.15x 1 m cross section allows the testing of two-dimensional flow phenomena. Wind tunnel data is summarised in Table 2. The flow field evaluation confirmed that the tunnel is suitable not only for educational, but also for certain scientific measurements [14].

The investigation was done in the smallest opened test section (0.35x0.35m) designated as "high speed". (According to Figure 4 the platform labelled as 12. was used instead of number 11. which is the closed test section).

The turbulence intensity (I) defined in (1) is 0.8% in the test section.

$$I = \frac{\sqrt{\overline{(u-\overline{u})^2}}}{|u|} \tag{1}$$

Where the numerator is the RMS (Root Mean Square) of the velocity and $\overline{u}$ is the mean velocity. The parameters are summarised in Table 3.

Table 3. Blackbird 1 wind tunnel parameters

	Size (WxHxL) [m]	Contraction ratio [-]	Max. test section velocity [m/s]
A	0.35×0.35×1	8.16	24
B	0.15×1×1	6.67	19.5
C	0.5×0.4×1	5	15

To maintain the Reynolds number of 33,750 the tests were conducted with 20.4 m/s velocity (measured dynamic pressure 250 Pa). The acting forces were measured with a two-component load cell. A Labview program was used to execute the measurements with the load cell connected to a PC through an NI PCI 6036E A/D converter. The dynamic pressure of the wind velocity was measured with a static Pitot tube connected to a

digital manometer (absolute error: 2 Pa). Angle of attack was controlled with a small servo actuator. The measurement setup can be seen on Figure 5.

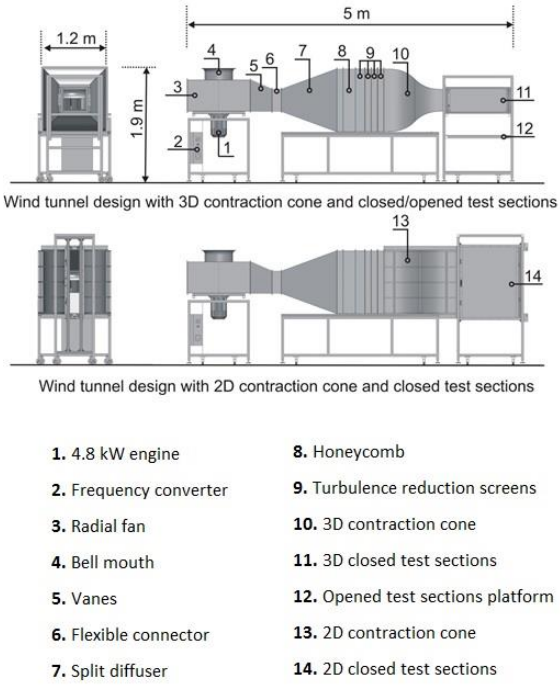

Figure 4. Wind tunnel layout and components. Top: with 0.35×0.35m test section. Bottom: with 1×0.15 m (2D) test section. Image courtesy of Gulyás et al. **[14]**.

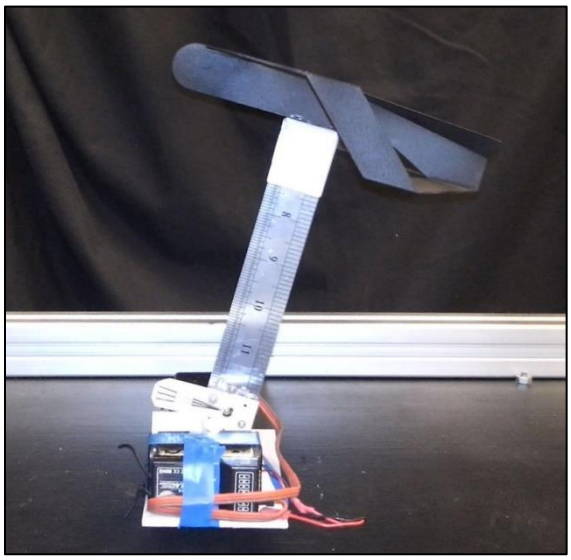

Figure 5. Test setup with the wind tunnel mock-up mounted upside down.

The measured forces were the lift (L) and drag (D) components of the aerodynamic force. The constant error of the load cell was derived from the calibration data along with the effect of the moving CG (Centre of Gravity) as function of the AOA.

Reynolds number is based on the chord (c), inlet reference velocity (u_{ref}). The velocity of the flow, used as reference velocity, was derived from pressure measurements on the calibrated inlet confusor. The blockage ratio at 6° angle of attack was 7.5% in the test section. The Mach number during the measurement was 0.03.

5. RESULTS

The DES and LES simulations were assessed after reaching 6 Flow-Through Number (FTN). Coefficients were time-averaged (example shown on Figure 6.) to be comparable with RANS and experimental data.

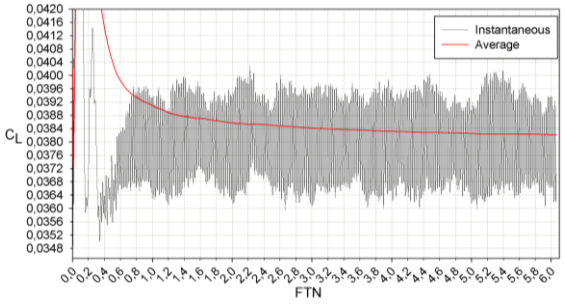

Figure 6. Convergence of the lift coefficient (c_L) for the half-aircraft in the 6° AOA DES simulation with the time-averaged coefficient (red), as a function of FTN.

Two series of measurements were conducted with 5-second and 10-second sampling times respectively. The results are summarised in Figure 7. This data is shown along with the simulation results in Figure 8 and Figure 9.

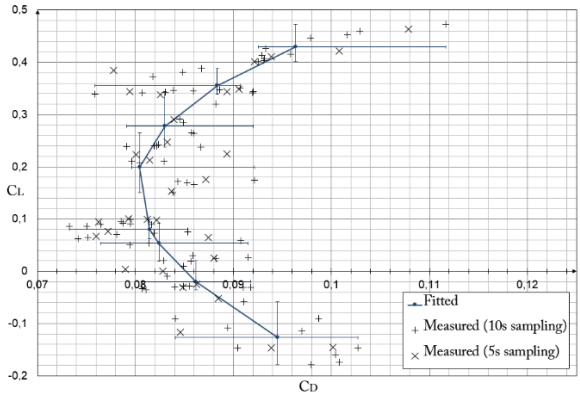

Figure 7. Measured polar diagram of the aircraft.

It can be seen on Figure 8 and Figure 9 that the LES and DES data obtained for 0° and 6° AOA are very close to each other with the difference in both parameters less than 0.6%.

The calculated lift coefficient and the experimental results are in good agreement, the drag coefficient, however does not match well the numerical results and the difference steadily increases with the AOA. In the -1 +1° AOA range, the calculated and measured parameters are within the error range of the study.

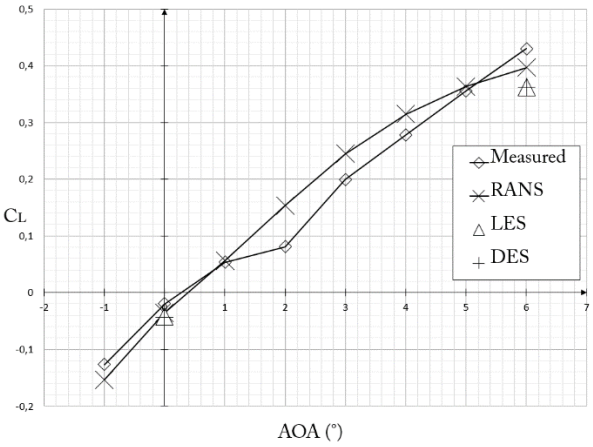

Figure 8. Lift coefficients as a function of the angle of attack (calculated and measured).

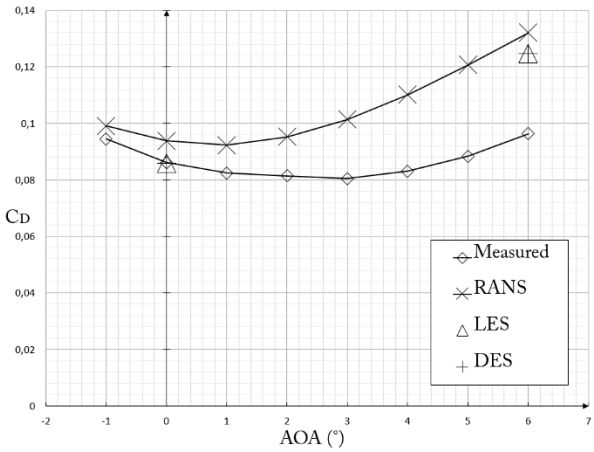

Figure 9. Drag coefficients as a function of the angle of attack (calculated and measured).

The pressure distribution on the wings are similar in each simulations case. The DES and LES methods show a negative pressure region near the trailing edge of the forward wing. The plots of pressure around the middle sections of both the forward and rearward wings are shown on Figure 10 and Figure 11 respectively.

The shear stress distributions reveal the well-resolved separation bubble downstream the leading edge, shown on Figure 12 and Figure 13.

The difference between results is further shown on Figure 14 and Figure 15 where the vortex system is visualised with isosurfaces of Q-criterion [15], colour-coded with the magnitudes of velocity. The comparison is at 0° and 6° AOA respectively and both the RANS results and the high-fidelity results are compared. The interaction between the lower- and upper wings can be observed in Figure 15.

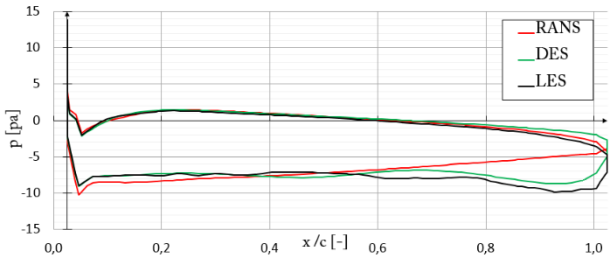

Figure 10. Pressure distribution around the profile at 6° AOA, mid-span, forward wing. The coordinates are relative to the chord length.

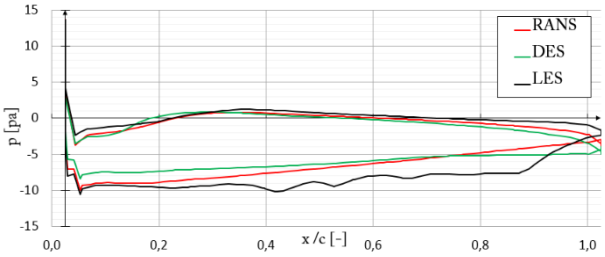

Figure 11. Pressure distribution around the profile at 6° AOA, mid-span, rear wing. The coordinates are relative to the chord length.

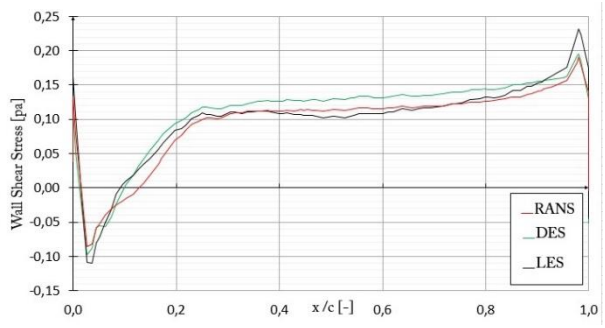

Figure 12. Shear stress distribution at 6° AOA, mid-span, forward wing. The coordinates are relative to the chord length.

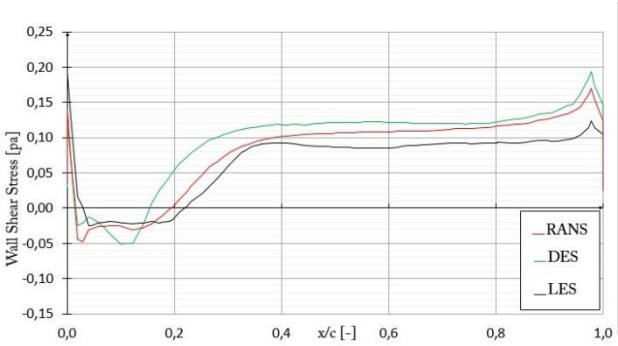

Figure 13. Shear stress distribution at 6° AOA, mid-span, rearward wing. The coordinates are relative to the chord length.

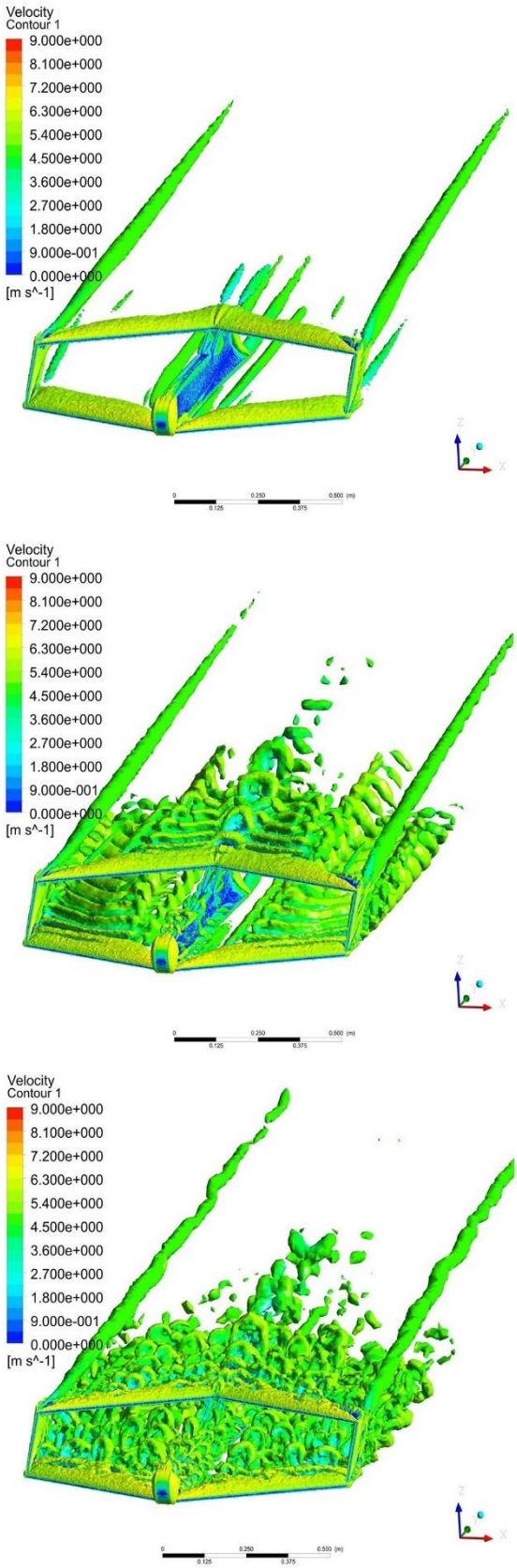

Figure 14. Q-criteria isosurfaces (Q=0.0014) with the contours of velocity magnitude for the RANS (top) DES (middle) and LES (bottom) simulations at 6° AOA.

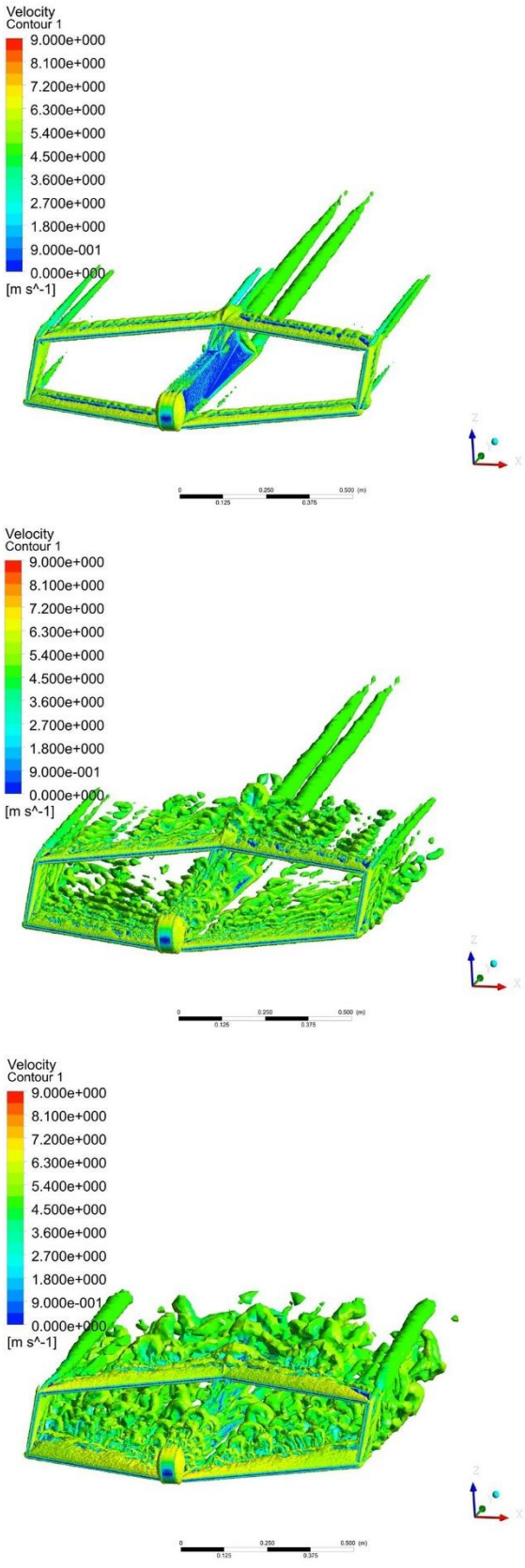

Figure 15. Q-criteria isosurfaces (Q=0.0014) with the contours of velocity magnitude for the RANS (top) DES (middle) and LES (bottom) simulations at 0° AOA.

6. CONCLUSIONS

In the present study, the CFD analysis of a box-wing aircraft using high fidelity numerical codes was presented.

Using an unstructured tetrahedral mesh a comparison between RANS, DES and LES models was made. While all of the models resolved the tip vortexes on the stabilisers and the vortexes originating from the ends of the wing connectors, the additional resolution of the DES and LES model yielded refined results comparable with the wind tunnel results at the lower AOA range.

The test aircraft used in this study is a rough prototype used to test out construction techniques and stability. A refined version is under development with proper airfoils and geometry using the experience acquired with the current vehicle.

The further evaluation of DES and LES techniques in this case is pending. The mesh sensitivity of the problem using structured hexahedral, polyhedral or hybrid meshed should also be studied. It is concluded that the computational requirements of this problem are moderate enough to be affordable for industrial application.

ACKNOWLEDGEMENTS

The authors would like to thank András Gulyás for his invaluable help with the wind tunnel measurements, Péter Rimóczi and Varinex co. ltd. for manufacturing the mock-up, and the Department of Fluid Mechanics for providing the computational power and wind tunnel time for this study.

The work relates to the scientific program of the project "Development of quality-oriented and harmonized R+D+I strategy and the functional model at BME", supported by the New Hungary Development Plan (Project ID: TÁMOP-4.2.1/B-09/1/KMR-2010-0002). It is also supported by the project "Talent care and cultivation in the scientific workshops of BME" project (Project ID: TÁMOP-4.2.2/B-10/1-2010-0009).

REFERENCES

[1] P. Jemitola és J. P. Fielding, „Box Wing Aircraft Conceptual Design," in *28th International Council of the Aeronautical Sciences*, Brisbane, 2012.

[2] D. Schiktanz és D. Scholz, „Box Wing Fundamentals - an Aircraft Design Perspective," in *Deutscher Luft- und Raumfahrtkongress*, Bremen, 2011.

[3] F. A. Khan, Preliminary Aerodynamic Investigation of Box-Wing Configurations using Low Fidelity Codes, MSc. Thesis, Kiruna: Lulea University of Technology, 2010.

[4] A. Frediani, "The Prandtl Wing," *VKI lecture series: "Innovative Configurations and Advanced Concepts for Future Civil Transport Aircraft",* 2005.

[5] A. Frediani, M. Gasperini, G. Saporito és A. Rimondi, „Development of a Prandtl plane aircraft configuration," in *Proceedings of the 17th AIDAA Congress*, Roma, 2003.

[6] P. R. Spalart, W. H. Jou, M. Strelets és S. R. Allmaras, „Comments on the feasibility of LES for wings, and on a hybrid RANS/LES approach," *Advances in DNS/LES*, %1. kötet1, pp. 4-8, 1997.

[7] M. Lesieur, O. Metais és P. Comte, „Large-eddy simulations of turbulence," *Cambridge university press*, 2005.

[8] P. Sagaut, „Large Eddy Simulation for Incompressible Flows," *Springer*, 2004.

[9] M. Germano, U. Piomelli, P. Moin és W. Cabot, „A Dynamic Subgrid-Scale Eddy Viscosity Model," *Physics of Fluids A: Fluid Dynamics*, %1. kötet3, %1. szám7, pp. 1760-1765, 1991.

[10] I. Celik, Z. Cehreli és I. Yavuz, „Index of resolution quality for Large Eddy Simulation," *Journal of Fluids Enfineering*, %1. kötet127, %1. szám5, pp. 949-958, 2005.

[11] L. Nagy, T. Régert és M. Lohász, „Large-Eddy Simulation in the vicinity of the RAF-6E airfoil in a reduced domain," in *In: XIX Polish National Fluid Dynamics Conference, KKMP2010*, Poznań, Poland, 5-9 September 2010, 2010.

[12] B. Geurts, Elements of direct and large eddy simulation, R.T. Edwards, 2004.

[13] P. R. Spalart, „Detached-eddy simulation.," *Annual Review of Fluid Mechanics 41*, pp. 181-202, 2009.

[14] A. Gulyás és M. Balczó, „Development of a Small Blower-type Wind Tunnel for Educational Purposes," in *28th microCAD International Multidisciplinary Scientific Conference*, Miskolc, 2014.

[15] G. Haller, „An objective definition of a vortex," *Journal of Fluid Mechanics*, %1. kötet525, pp. 1-26, 2005.

[16] M. Shur, P. R. Spalart, M. Strelets és A. Travin, „Detached-eddy simulation of an airfoil at high angle of attack," *Engineering turbulence modelling and experiments*, %1. kötet4, pp. 669-678, 1999.